Erzincan Üniversitesi
Fen Bilimleri Enstitüsü Dergisi
2021, 14(1), 241-248
ISSN: 1307-9085, e-ISSN: 2149-4584
Araştırma Makalesi

Erzincan University
Journal of ScienceandTechnology
2021, 14(1), 241-248
DOI: 10.18185/erzifbed.877769
Research Article

Elastic Scattering with Double Folding Model: $^{8}B+^{27}Al$

Yusuf SERT[1*]

[1]Yozgat Bozok Üniversitesi, Sorgun Meslek Yüksekokulu, Yozgat, Türkiye

Geliş / Received: 09/02/2021, Kabul / Accepted: 02/03/2021

Abstract

In the present work, the elastic scattering of the 8B+27Al reaction at two different energies have been examined using the microscopic double folding potential approximation within the framework of the optical model. The real part of the optical model has been obtained by using Fermi, Gaussian and Variational Monte Carlo (VMC) density distributions in the microscopic double folding model and the imaginary part has been taken as Woods-Saxon volume type. The results of our microscopic analysis are quite compatible with the experimental cross-section data. The reaction cross sections, the volume integrals of used potentials and their χ2/N errors have also been computed. This study is important in showing the effect of microscopically derived potentials in explaining the 8B+27Al experimental data published recently.

Keywords: Double folding, proton halo nuclei, elastic scattering

Çift Katlama Modeli İle Elastik Saçılma: $^{8}B+^{27}Al$

Öz

Bu çalışmada, $^{8}B+^{27}Al$ reaksiyonunun iki farklı enerjide elastik saçılması, optik model çerçevesinde mikroskobik double folding potansiyeli yaklaşımı kullanılarak incelenmiştir. Optik modelin reel kısmı mikroskobik double folding modelde Fermi, Gaussian ve Variational Monte Carlo (VMC) yoğunluk dağılımları kullanılarak elde edilmiş ve imajiner kısım Woods-Saxon hacim tipi olarak alınmıştır. Mikroskobik analizimizin sonuçları, deneysel tesir kesit verileri ile oldukça uyumludur. Reaksiyon tesir kesitleri, kullanılan potansiyellerin hacim integralleri ve bunların χ2/N hataları da hesaplanmıştır. Bu çalışma, son zamanlarda yayınlanan $^{8}B+^{27}Al$ deneysel verilerini açıklamada mikroskobik olarak türetilmiş potansiyellerin etkisini göstermesi açısından önemlidir..

Anahtar Kelimeler: Double folding, proton halo çekirdek, elastik saçılma

1. Introduction

The radioactive ion beam (RIB) facilities have opened a way for significant improvements in the field of nuclear physics, especially those related to the halo nuclei. Structurally halo has tightly bound core with weakly bounded valence nucleons. The half-lives of these extraordinary nuclei are usually very short. Halo nuclei are evaluated in two groups; these are neutron and proton halos. These nuclei are evaluated according to their state in the stability valley. The most common proton halo is the ^{8}B nuclei which has low break up threshold. The ^{8}B nuclei has a weakly bound proton with a proton separation energy S_p =0.137 MeV and its half-life is $t_{1/2}$=770 ms. Nuclear reactions and densities involving short-lived ^{8}B nuclei have been extensively investigated by both nuclear astrophysicists, experimental and theoretical nuclear physicist (Aguilera et al., 2011; Aguilera, Martinez-Quiroz, Belyaeva, Kolata, & Leyte-Gonzalez, 2008; Aguilera et al., 2009; Aguilera, Martinez-Quiroz,

*Corresponding Author: yusufsert1984@yahoo.com.tr

Rosales, et al., 2008; Barioni et al., 2011; Camacho, Aguilera, Gomes, & Lubian, 2011; Camacho, Aguilera, Lubian, & Gomes, 2013; Carlson et al., 2015; Chandel, Dhiman, & Shyam, 2003; Horii, Takashina, Furumoto, Sakuragi, & Toki, 2010; Lubian et al., 2009; Lubian & Nunes, 2007; Mackintosh & Pang, 2013; Mitchell et al., 2010; Morcelle et al., 2017; Moro, Crespo, Nunes, & Thompson, 2002; Varga, Suzuki, & Tanihata, 1995; Yang et al., 2013). In the theoretical analysis microscopic and phenomenological potential approximations have been used in explaining the measured experimental data. The theoretical models attempt to clarify the elastic and inelastic scattering data as well as other observables such as fusion, S-factor and total reaction cross-section data. In order to clarify the measured experimental cross-section data, these models range from optical model to coupled-channels using continuum discretized coupled channels (CDCC) formalism with phenomenological as well as microscopic potentials polarization potential.

Recently, Morcelle (Morcelle et al., 2017) et al. have measured new experiment for the 8B+27Al elastic scattering. The experiment is conducted in the Radioactive Ion Beams in Brasil facility (RIBRAS) in São Paulo, and in the TwinSol facility at the University of Notre Dame, USA above the Coulomb barrier at energies of E_{lab}=15.3 and 21.7 MeV. The angular distributions were measured in the angular range of 15–80 degrees. They have investigated the experimental data theoretically by using two different types of optical potentials.

Therefore, in this paper, we have investigated the same $^{8}B+^{27}Al$ elastic scattering angular distribution by using microscopic double folding potentials within the framework of optical model. Our aim is to show the effect of microscopic potentials in clarifying the experimental cross-section data of the $^{8}B+^{27}Al$ system around and above the Coulomb barrier.

In the next part, we present our theoretical model and the microscopic potentials obtained with different nuclear matter density distributions. In Section 3, we present the results of optical model calculations performed by using these two different potentials. Our conclusion is given in Section 4.

2. Theoretical Analysis

The interaction between two nuclei is generally defined as a many-body problem, and many reactions can occur as a result of this interaction. These are elastic scattering, inelastic scattering, nucleon transfer reactions and projectile fragmentations. The shape of these reactions is determined by the structure of projectile and the incoming energy, and the simplest of these reactions is the elastic scattering. Within mean-field approximation, the elastic scattering is described by using the optical model approach with either phenomenological potentials such as Woods-Saxon or Woods-Saxon derivatives or microscopic-double folding (DF) potentials. In literature, the interaction of the projectile and target nuclei is defined as optical model. The identified potential in this model has a Coulomb, centrifugal and nuclear interactions parts. In the elastic reaction, the real and imaginary parts of the nuclear potential are responsible for scattering and the lost flux, respectively (Aygun, Kocadag, & Sahin, 2015; Brandan & Satchler, 1997; Satchler, 1983). In this study, all of the computations and comments have been made according to the Microscopic Model-Double Folding method (DF). DF model is the most popular procedure for analyzing experimental angular distributions of halo nuclei on stable nuclei. In microscopic model, while imaginary potential is taken Woods-Saxon or Woods-Saxon square type potential, the real potential can be defined using double folding model.

In double folding model, the density distributions of both the projectile and target nuclei are used. The elastic scattering of ^{8}B as one-proton halo nucleus on ^{27}Al target was examined using the double folding model within the framework of the OM at the incident energies, E_{Lab}=15.3 MeV and E_{Lab}=21.7 MeV. The total effective potential is given in Equation 1.

$$V_{total}(r) = V_{Coulomb}(r) + V_{Nuclear}(r) + V_{Centrifugal}(r) \qquad (1)$$

In this equation the Coulomb potential term (Satchler, 1983) is owing to the interaction between the projectile and target in proton (charge) numbers over a sphere of radius R_c (Equation 2).

$$V_{Coulomb}(r) = \frac{1}{4\pi\varepsilon_0}\frac{Z_P Z_T e^2}{r} \quad r \geq Rc \qquad (2)$$

$$= \frac{1}{4\pi\varepsilon_0}\frac{Z_P Z_T e^2}{2Rc}\left(3 - \frac{r^2}{Rc^2}\right) \quad r < Rc$$

Similarly, the radius of Coulomb interaction is taken as $Rc = 1.10(A_P^{1/3} + A_T^{1/3})$ fm, Z_P and Z_T describe the charges of the projectile and target nuclei, one by one. The centrifugal potential is given as Equation 3.

$$V_{centrifugal}(r) = \frac{\hbar^2 l(l+1)}{2\mu r^2} \qquad (3)$$

where μ is the reduced mass of the interaction (^{8}B-^{27}Al) and l is angular momentum, r is radius and h is Planck constant, respectively. The final term of the total potential is the complex nuclear potential $V_{Nuclear}(r)$ described as the double folding potential. This term with V_{NN} an effective nucleon-nucleon interaction potential could be given as shown in Equation 4.

$$V_{DF}(r) = \int dr_1 \int dr_2\, \rho_P(r_1)\rho_T(r_2)V_{NN}(r_{12}) \quad (4)$$

where $\rho_P(r_1)$ and $\rho_T(r_2)$ are the nuclear matter densities of projectile and target nuclei, respectively. We have benefited from three different matter density distributions for the ^{8}B halo nucleus in both ground state and 2^+ ground state (in VMC) to make a comparison work. The first density is 3-parameters Fermi distribution and the second density is Gaussian distribution in our analysis for the ^{8}B proton halo nucleus (Equation 5 and 6).

$$\rho(r) = \frac{\rho_0}{\left[1+exp\left(\frac{r-c}{a}\right)\right]}: \text{ Fermi distribution for projectile nuclei} \quad (5)$$

where $\rho_0 = 0.1507\ (fm^{-3})$, $c = 2.000\ (fm)$

and $a = 0.486\ (fm)$;

$$\rho(r) = Cexp\left[-\left(\frac{r}{a}\right)^2\right]: \text{ Gaussian distribution for projectile nuclei} \quad (6)$$

where $\rho_0 = 0.159177\ (fm^{-3})$, $\alpha = 2.08207\ fm$; these coefficients can be found in normalization condition (Equation 7).

$$4\pi \int \rho(r) r^2 dr = 8\ (A_P) \qquad (7)$$

here A is the mass number for the projectile nucleus (^{8}B). These density distributions give a root mean square (rms) radius-experimental value of 2.380 fm (Tanihata et al., 1985; Tanihata et al., 1988). For the projectile (8B), used third density distribution is the VMC which is taken from the VMC calculations using the Argonne v18 (AV18) two-nucleon and Urbana X three-nucleon potentials (AV18+UX). The proton and neutron rms values have been obtained with this method as 2.4482 fm and 2.1389 fm, respectively. When the density distributions are normalized, the nucleons number of protons and neutron is obtained 4.9977 and 2.9981, respectively (Carlson et al., 2015).

For ^{27}Al nucleus, the nuclear matter density has been obtained from RIPL-3 (Capote et al., 2009). Both the projectile and target nucleus density distributions have been displayed in Figure 1 (a), Figure 1 (b) and Figure 1 (c) in logarithmic form.

The effective nucleon-nucleon potential term consists of 3 components. The first part in Equation 8 is realistic interaction parameters. We have used the most general one, the M3Y nucleon-nucleon (Michigan 3 Yukawa) realistic interaction (Brandan & Satchler, 1997; Khoa, Satchler, & Von Oertzen, 1995).

$$V_{NN}(r) = 7999\frac{\exp(-4r)}{4r} - 2134\frac{\exp(-2.5r)}{2.5r} + J_{OO}(E)\delta(r)\ (MeV) \qquad (8)$$

The second term in the Equation 8 is $J_{OO}(E - \text{linear energy dependence})$. This term represents the nucleon exchange term (Equation 9).

$$J_{OO}(E) = -276\left[1 - \frac{0.005E_{Lab}}{A_P}\right] MeV fm^3 \qquad (9)$$

The DF potentials are obtained using the double folding computer code DFPOT (Cook, 1982). By using this double-folding approach, we have obtained the real part of the nuclear potential with these three different distributions. The shapes of the real part of the potential are shown in Figure 2. As it can be seen from Figure 2, the produced real potential with the Fermi distribution is deeper than the potential produced by using both the Gaussian distribution and VMC density distribution in the double-folding model at the same energies. In Figure 2, the calculated folding potentials of $^{8}B+^{27}Al$ cannot be distinguished from each other especially the far periphery region 5-10 fm, the most important one when estimating cross sections. For this reason the graph was drawn in logarithmic form to see better, and also the net shapes of the potentials have been given on the side as (a) and (b)-two different graphics.

Figure 1. The density distribution of ^{8}B (a)-(b) and ^{27}Al (c) nuclei in logarithmic form.

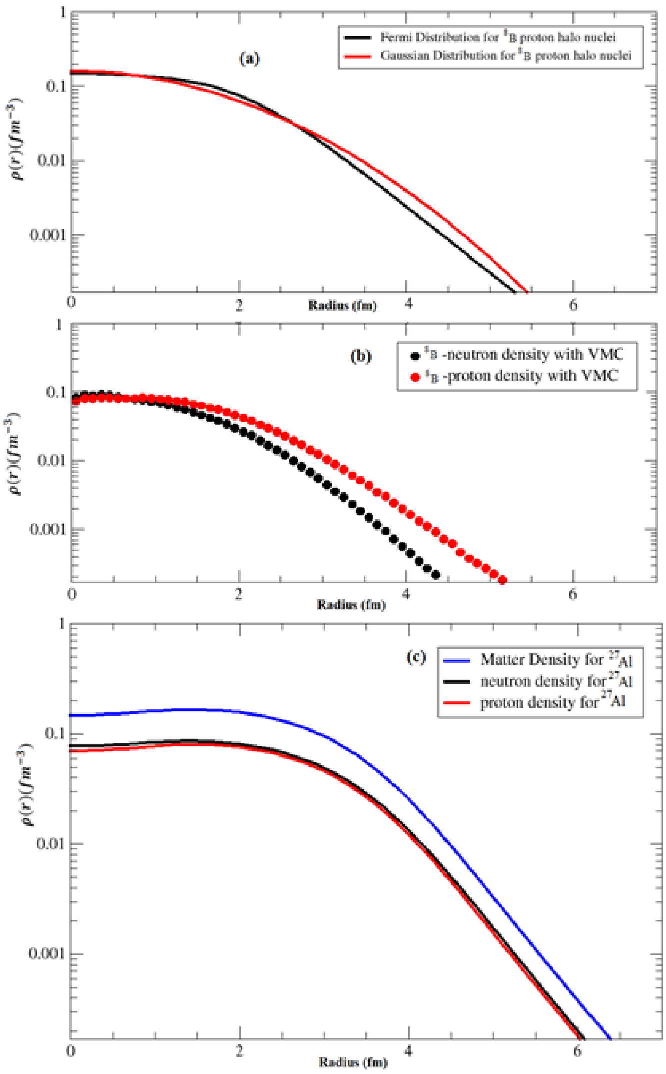

While the real part of the optical model is obtained by using the above-described double folding model, the imaginary potential is taken as in the form of Wood-Saxon shape in Equation 10 as following,

Figure 2. The shapes of the real potential of the nuclear potential of ^{8}B which interacts with ^{27}Altarget nuclei at 15.3 and 21.7 MeV.

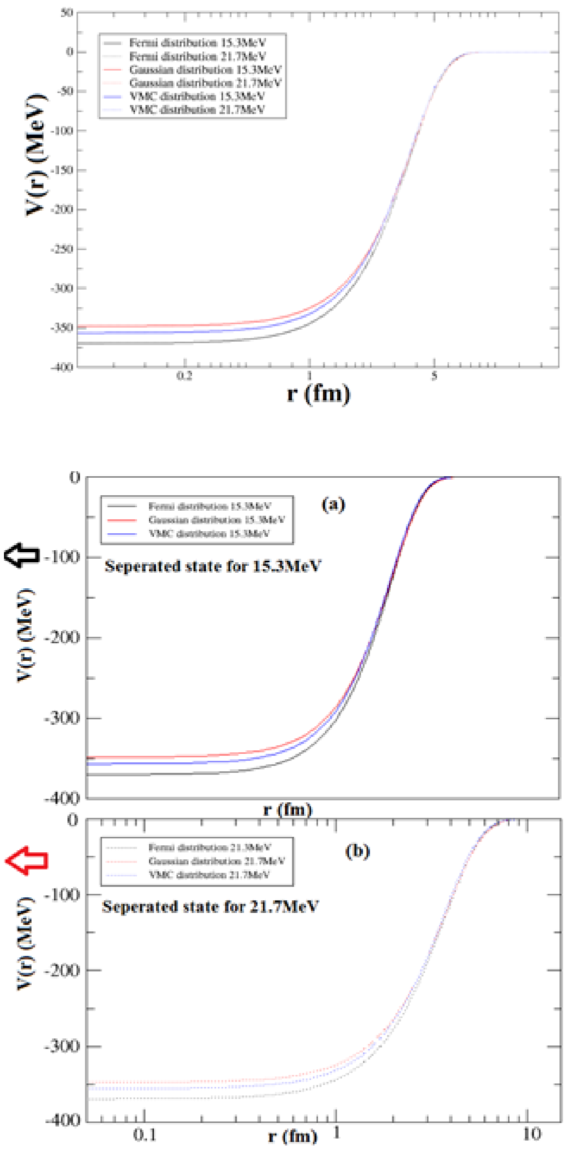

$$W(r) = \frac{W_0}{\left[1 + exp\left(\frac{r-R_W}{a_W}\right)\right]} \qquad (10)$$

where $R_W = r_W(A_P^{\frac{1}{3}} + A_T^{1/3})$ and A_P and A_T are mass numbers of the projectile-^{8}B and target nuclei-^{27}Al, respectively. Consequently total nuclear potential can be expressed as shown in Equation 11.

$$V_N(r) = N_R V_{DF}(r) - i\frac{W_0}{\left[1 + exp\left(\frac{r-R_W}{a_W}\right)\right]} \qquad (11)$$

where N_R is the normalization factor of the produced potential. All obtained parameters have been displayed as in Table 1. The FRESCO code (Thompson, 1988) has been handled to investigate the parameters of optical model via assembling with the experimental data

Table 1. The OM parameters used in microscopic model analysis of $^{8}B+ ^{27}Al$ reaction

Elab (MeV)	Distribution Type	N_R factor	W_0 (MeV)	r_w (fm)	a_w (fm)	σ mb	J_v $MeV.fm^3$	J_w $MeV.fm^3$	χ2/N
15.3	Fermi	1.0	19.7	1.4	0.67	557	418.701	139.146	0.034396
	Gaussian	1.0	19.7	1.4	0.67	569	418.625	139.146	0.034698
	with VMC	1.0	19.7	1.4	0.67	551	394.486	139.146	0.033916
21.7	Fermi	1.0	34.7	1.4	0.67	1312	417.598	245.094	0.460984
	Gaussian	1.0	34.7	1.4	0.67	1321	417.522	245.094	0.436861
	with VMC	1.0	34.7	1.4	0.67	1307	393.446	245.094s	0.479018

3. Results and Discussion

The $^{8}B+ ^{27}Al$ reaction data has been recently measured (Morcelle et al., 2017) and there has been no study by using a double-folding potential with different densities to explain this experimental data. Therefore, we have studied the elastic scattering of the ^{8}B nucleus from ^{27}Al target nucleus at above the Coulomb barrier within the framework of the above-described double folding model. The microscopic potential has been generated by using three different nucleon matter densities- Fermi, Gaussian and VMC density distributions for the ^{8}B-the lowest energy state. The real part of the potential is shown in Figure-2 for Fermi, Gaussian and VMC density distributions. The imaginary part of the optical potential is taken as Wood-Saxon form and the best fit parameters with double-folding potential, reaction cross-sections, volume integrals and χ2/N values for two energies are shown in Table-1. The results are presented in Figure-3 and Figure-4. As it can be seen from these figures, our microscopic potentials obtained by using Fermi, Gaussian and VMC density distributions provide very well compromise with the experimental scores and generates successfully the minimums and maximums of the elastic scattering at two different energies. The treatment of the cross-sections generated by Fermi, Gaussian and VMC density distributions are very similar at both forward and backward angles. From Table-1, we have observed that both 15.3MeVand 21.7MeV incoming energies the largest cross-section is 569 mb and 1321 mb, respectively in Gaussian distribution. On the other hand; we have observed that for 15.3MeV, with VMC obtained error results are better than the result of Fermi and Gaussian distribution, but for 21.7MeV with Gaussian distribution obtained error results are better than the results of Fermi and VMC density distributions. Some times it may be difficult to evaluate according to the results of $\chi2/N$, we may come across with interpretations of these results in the literature (Farag, Esmael, & Maridi, 2014).

In the double-folding model, free parameter is the normalization constant N_R. As shown in Table-1, we kept this value as constant to examine the behavior of the imaginary potential. As the energy of the projectile in the reaction is increased, it is expected that the flux from the elastic channel would be removed to the other channels due to the occurrence of inelastic. Therefore, as the energy increases, we expect an increase at the depth of the imaginary potential. This is what we have exactly observed in our potential parameters. As it can be seen from Table-1, while energy of ^{8}B is 15.3 MeV, the depth of imaginary potential is 19.7 MeV, as the energy increases to E_{lab}=21.7, the depth of imaginary potential increases to 34.7 MeV. Our finding is in very good agreement with the expectation. With this fixed real and energy dependent imaginary potentials, we have also obtained total reaction cross section and volume integrals of the real and imaginary parts of the optical potential at two energies. It should be emphasized that our results are in agreement with the findings of Morcelle et al. (Morcelle et al., 2017). Finally, as shown in Table-1, we have computed the volume integrals of the potentials used to describe for the $^{8}B+^{27}Al$ elastic scattering by using following equations:

$$J_V = \frac{4\pi}{A_P A_T}\int V(r,E) r^2 dr \qquad (12)$$

$$J_W = \frac{4\pi}{A_P A_T}\int W(r,E) r^2 dr \qquad (13)$$

where A_P is the mass number of the projectile, and A_T is the mass number of the target nucleus.

Figure 3. Angular distributions for the $^{8}B+^{27}Al$ elastic scattering at E_{Lab}=15.3 MeV.

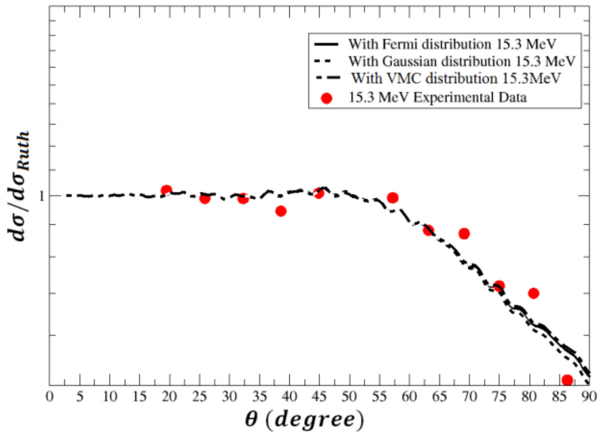

Figure 4. Angular distributions for the $^{8}B+^{27}Al$ elastic scattering at E_{Lab}=21.7 MeV.

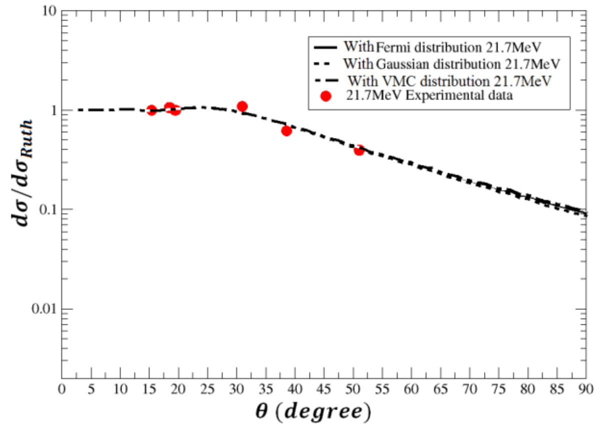

4. Conclusion

In this study, a theoretical analysis have been conducted for the first time by using Fermi, Gaussian and VMC density distributions for the elastic scattering of the $^{8}B+^{27}Al$ system at E_{Lab}=15.3 and 21.7 MeV. The real part of the complex optical potential is derived from the Fermi, Gaussian and VMC density distributions of the proton halo projectile ^{8}B and target ^{27}Al nuclei within double-folding potential model. The imaginary part of the potential has been taken as the form of

Woods-Saxon volume. Both at 15.3MeVand 21.7MeV, it has been noticed that the real potential of $^{8}B+^{27}Al$ (with Gaussian distribution) goes to zero faster than the other real potentials. However, we can express that the real potential of $^{8}B+^{27}Al$ (with Fermi distribution) is deeper than the other real potentials. We have investigated the effect of potentials of the elastic and reaction cross-sections as well as the change on the volume integrals of the potentials for two energies. We have shown that microscopic potentials obtained by using Fermi, Gaussian and VMC density distributions provide very good agreement with the experimental data.

Acknowledgments

Professor Dr. Jesus Lubian Rios (Instituto de Fisica Universidade Federal Fluminense), Professor Dr. Gamal El-Hiti (King Saud University) and Dr. M. Aygun (Bitlis Eren University) are greatly acknowledged for valuable comments on the manuscript. Also, the authors thank the R. B. Wiringa (Physics Division, Argonne National Laboratory, Argonne, USA) for providing the Variational Monte Carlo density distribution of $^{8}B(2^{+})$ nuclei.

References

Aguilera, E., Amador-Valenzuela, P., Martinez-Quiroz, E., Lizcano, D., Rosales, P., García-Martínez, H., . . . Lamm, L. (2011). Near-Barrier Fusion of the B 8+ Ni 58 Proton-Halo System. *Physical review letters*, *107*(9), 092701.

Aguilera, E., Martinez-Quiroz, E., Belyaeva, T., Kolata, J., & Leyte-Gonzalez, R. (2008). New measurements on breakup of 8 B+ 58 Ni at energies around the coulomb barrier. *Physics of Atomic Nuclei, 71*(7), 1163-1167.

Aguilera, E., Martinez-Quiroz, E., Lizcano, D., Gómez-Camacho, A., Kolata, J., Lamm, L., . . . Becchetti, F. (2009). Reaction cross sections for B 8, Be 7, and Li 6+ Ni 58 near the Coulomb barrier: Proton-halo effects. *Physical Review C*, *79*(2), 021601.

Aguilera, E., Martinez-Quiroz, E., Rosales, P., Lizcano, D., Gómez-Camacho, A., Kolata, J., . . . Camargo, O. (2008). Elastic scattering of a proton-halo nucleus: 8B+ 58Ni. *Revista mexicana de física, 54*, 1-4.

Aygun, M., Kocadag, O., & Sahin, Y. (2015). Phenomenological and microscopic model analysis of elastic scattering reactions of 18O by 24Mg, 28Si, 58Ni, 64Zn, 90Zr, 120Sn, and 208Pb target nuclei. *Revista mexicana de física, 61*(6), 414-420.

Barioni, A., Zamora, J., Guimaraes, V., Paes, B., Lubian, J., Aguilera, E., . . . Villano, A. (2011). Elastic scattering and total reaction cross sections for the B 8, Be 7, and Li 6+ 12 C systems. *Physical Review C*, *84*(1), 014603.

Brandan, M.-E., & Satchler, G. R. (1997). The interaction between light heavy-ions and what it tells us. *Physics reports, 285*(4-5), 143-243.

Camacho, A. G., Aguilera, E., Gomes, P., & Lubian, J. (2011). Breakup threshold anomaly for the 8 B+ 58 Ni system at near-Coulomb barrier energies. *Physical Review C, 84*(3), 034615.

Camacho, A. G., Aguilera, E., Lubian, J., & Gomes, P. (2013). Simultaneous $\chi 2$-analysis of near-barrier fusion and elastic scattering for the proton-halo system 8B+ 58Ni using dynamical Woods–Saxon polarization potentials. *Journal of Physics G: Nuclear and Particle Physics*, *40*(3), 035103.

Capote, R., Herman, M., Obložinský, P., Young, P., Goriely, S., Belgya, T., . . . Plujko, V. A. (2009). RIPL–reference input parameter library for calculation of nuclear reactions and nuclear data evaluations. *Nuclear Data Sheets*, *110*(12), 3107-3214.

Carlson, J., Gandolfi, S., Pederiva, F., Pieper, S. C., Schiavilla, R., Schmidt, K., & Wiringa, R. B. (2015). Quantum Monte Carlo methods for nuclear physics. *Reviews of Modern Physics, 87*(3), 1067.

Chandel, S., Dhiman, S., & Shyam, R. (2003). Structure of B 8 and astrophysical S 17 factor in Skyrme Hartree-Fock theory. *Physical Review C, 68*(5), 054320.

Cook, J. (1982). DFPOT-a program for the calculation of double folded potentials. *Computer Physics Communications, 25*(2), 125-139.

Farag, M., Esmael, E., & Maridi, H. (2014). Energy-dependent microscopic optical potential for scattering of nucleons on light nuclei. *The European Physical Journal A, 50*(6), 1-10.

Horii, K., Takashina, M., Furumoto, T., Sakuragi, Y., & Toki, H. (2010). Elastic scattering of B 8 from C 12 with internal three-cluster structure of B 8. *Physical Review C, 81*(6), 061602.

Khoa, D. T., Satchler, G., & Von Oertzen, W. (1995). Folding analysis of the elastic Li 6+ 12 C scattering: Knock-on exchange effects, energy dependence, and dynamical polarization potential. *Physical Review C, 51*(4), 2069.

Lubian, J., Correa, T., Aguilera, E., Canto, L., Gomez-Camacho, A., Quiroz, E., & Gomes, P. (2009). Effects of breakup couplings on B 8+ Ni 58 elastic scattering. *Physical Review C, 79*(6), 064605.

Lubian, J., & Nunes, F. (2007). Searching for a polarization potential in the breakup of 8B. *Journal of Physics G: Nuclear and Particle Physics, 34*(3), 513.

Mackintosh, R., & Pang, D. (2013). Significant features of 8 B scattering from 208 Pb at 170.3 MeV. *Physical Review C, 88*(1), 014608.

Mitchell, J., Rogachev, G., Johnson, E., Baby, L., Kemper, K., Moro, A., . . . Wiedenhöver, I. (2010). Low-lying states in B 8. *Physical Review C, 82*(1), 011601.

Morcelle, V., Lichtenthäler, R., Lépine-Szily, A., Guimarães, V., Pires, K., Lubian, J., . . . Becchetti, F. (2017). B 8+ Al 27 scattering at low energies. *Physical Review C, 95*(1), 014615.

Moro, A., Crespo, R., Nunes, F., & Thompson, I. (2002). 8 B breakup in elastic and transfer reactions. *Physical Review C, 66*(2), 024612.

Satchler, G. (1983). Int. series of monographs on Physics: Oxford University Press, Direct Nuclear reactions.

Tanihata, I., Hamagaki, H., Hashimoto, O., Shida, Y., Yoshikawa, N., Sugimoto, K., . . . Takahashi, N. (1985). Measurements of interaction cross sections and nuclear radii in the light p-shell region. *Physical review letters, 55*(24), 2676.

Tanihata, I., Kobayashi, T., Yamakawa, O., Shimoura, S., Ekuni, K., Sugimoto, K., . . . Sato, H. (1988). Measurement of interaction cross sections using isotope beams of Be and B and isospin dependence of the nuclear radii. *Physics Letters B, 206*(4), 592-596.

Thompson, I. J. (1988). Coupled reaction channels calculations in nuclear physics. *Computer Physics Reports, 7*(4), 167-212.

Varga, K., Suzuki, Y., & Tanihata, I. (1995). Microscopic four-cluster description of the mirror nuclei Li 9 and C 9. *Physical Review C, 52*(6), 3013.

Yang, Y., Wang, J., Wang, Q., Pang, D., Ma, J., Huang, M., . . . Bai, Z. (2013). Elastic scattering of the proton drip-line nucleus 8 B off a nat Pb target at 170.3 MeV. *Physical Review C, 87*(4), 044613.